Sensing with toroidal metamaterial

Gupta, Manoj; Srivastava, Yogesh Kumar; Manjappa, Manukumara; Singh, Ranjan

2017

Sensing with toroidal metamaterial

Manoj Gupta,[1,2] Yogesh Kumar Srivastava,[1,2] Manukumara Manjappa,[1,2] and Ranjan Singh[1,2,a]

[1]*Division of Physics and Applied Physics, School of Physical and Mathematical Sciences, Nanyang Technological University, Singapore 637371*
[2]*Centre for Disruptive Photonic Technologies, The Photonics Institute, Nanyang Technological University, 50 Nanyang Avenue, Singapore 639798*

Localized electromagnetic excitation in the form of toroidal dipoles has recently been observed in metamaterial systems. The origin of the toroidal dipole lies in the currents flowing on the surface of a torus. Thus, the exotic toroidal excitations play an important role in determining the optical properties of a system. Toroidal dipoles also contribute towards enabling high quality factor subwavelength resonances in metamaterial systems which could be an excellent platform for probing the light matter interaction. Here, we demonstrate sensing with toroidal resonance in a two-dimensional terahertz metamaterial in which a pair of mirrored asymmetric Fano resonators possesses anti-aligned magnetic moments at an electromagnetic resonance that gives rise to a toroidal dipole. Our proof of concept demonstration opens up an avenue to explore the interaction of matter with toroidal multipoles that could have strong applications in the sensing of dielectrics and biomolecules. *Published by AIP Publishing.* [http://dx.doi.org/10.1063/1.4978672]

Over a long period of time, light matter interaction has attracted tremendous attention of the scientific community and has emerged as a powerful tool to manipulate the electromagnetic (EM) response of matter for almost the entire range of EM radiation. Several kinds of light matter interaction based electromagnetic devices are currently being employed in the area of telecommunication, imaging, healthcare, and defence industry. Metamaterials, which are the composite array of sub-wavelength structures, are one such kind of devices that offer novel effects by controlling the response that originates from the interaction between meta-atoms and electromagnetic radiation.[1–3] Remarkable functionalities such as slow light effects,[4] negative refraction,[5] super lenses,[6] invisibility cloaks,[7,8] and sensing have been demonstrated using metamaterial based devices.[9–12] The unique advantage of the metamaterial structure is to support electromagnetic resonance at a specific frequency based on its structural size. Such a unique tuning ability can strengthen the adaptability of the metamaterial based electromagnetic devices in the near future.

Promising applications offered by metamaterial device designs are very much dependent on their performance. The low performance of these kinds of devices is mainly due to the radiative and non-radiative losses encountered in these systems.[13] Several schemes have been demonstrated to overcome the losses such as by optimizing the shape and size of the sub-wavelength structure in the unit cell of the metasurface,[14–18] by using a low loss superconductor, and by introducing a gain medium.[19,20] The performance of all metamaterials and plasmonic based devices would certainly be enhanced by overcoming the losses. One of the direct device applications of metamaterials is that of a sensor at optical,[10,21] infrared,[22,23] and terahertz (THz) frequencies.[24,25] In recent times, among different frequency bands,

terahertz sensing has received a lot of attention due to its remarkable scientific and technological abilities in multidisciplinary fields.[26,27] For ultrasensitive sensing applications, there is a requirement of high quality (Q) factor resonances that have extremely narrow bandwidth. Moreover, the amplitude of resonance should be strong enough so that it is easier to detect them in a noisy environment. The resonances supported by metamaterial structures respond to the changes in the effective refractive index of the medium at its surface.[28,29] Thus, metamaterials provide a robust sensing platform since they could be easily fabricated on different types of thin substrates, which can also be flexible in nature.[30,31]

In this article, we have performed terahertz domain refractive index sensing with toroidal dipolar resonance in planar metamaterials, which is easy to fabricate in a single step photolithography cycle. In the metamaterial system, the toroidal dipolar response was first demonstrated at the microwave regime by using the metasurface composed of 3D meta-molecule structures.[32] It was recently discovered that even planar metasurfaces could support strong toroidal resonances, which are high-Q in nature, and could provide sufficiently large field confinement necessary for sensing applications.[33–36] The overall response of the metamaterial array can be seen as the contribution due to different multipoles, where contribution due to the specific toroidal multipole can be analytically computed by multipole analysis.[37–39] In a two-dimensional metasurface, the toroidal response can be excited by using the symmetry broken split ring resonator also known as asymmetric split ring resonator or Fano resonator.[36,40] The metamolecule array of the toroidal metasurface consists of a mirrored Fano resonator pair that is coupled through toroidal moment during electromagnetic excitation due to anti-aligned set of magnetic dipoles.[36] In the planar metasurface, the mirrored asymmetric resonator array, having similar degree of asymmetry, possesses significantly higher Q and figure of merit (FoM) values for toroidal resonance compared to the

a)ranjans@ntu.edu.sg

traditional Fano resonator array.[15,36] High Q toroidal resonances support strong interaction between the electromagnetic wave and a specific analyte. A minute quantity of analyte on the metasurface results in very small spectral shifts of toroidal resonance, which allows the detection of the dielectric medium or biological local environment near the metasurface. Additionally, sharp toroidal resonance offers better sensing performance compared to broad resonances, which typically lack the ability to detect small spectral shifts in the resonance frequency.[41,42] Thus, high-Q toroidal metasurface offers another important sensing platform with enhanced sensitivities which could give rise to an excellent photonic device for highly sensitive dielectric, chemical, liquid, and biological sensing applications.[43–47]

We performed terahertz time domain spectroscopy (THz-TDS) to measure the sensing parameters of the high-Q planar toroidal metasurface. A close agreement between simulated and experimental response substantiates the role of toroidal resonance in THz sensing. Figure 1(a) shows the diagrammatic image of the terahertz asymmetric split ring resonator (TASR), which consists of a double split gap square shaped metallic strip. The outer dimension of individual resonator is 60 μm × 60 μm, with the arm width of 6 μm and the split-gap size equal to 3 μm. The asymmetric nature of the TASR structure is due to positioning of both the split gaps, which are located 9 μm away from the centre of the

resonator. The TASR metamaterial samples were fabricated on the high-resistivity (4 kΩ–cm), p-type silicon (0.5-mm thick) substrate using photolithography followed by deposition of a 200-nm thick aluminium (Al) film in a thermal evaporator. During the experiments, a high-resistivity (4 kΩ–cm), 10-mm thick silicon plate was used for an optical contact behind the metamaterial surface to eliminate the Fabry Perot reflection from the back surface of the substrate, which enabled a scan length of 60 ps in the time domain, providing a measurement frequency resolution of 16.6 GHz. For the excitation of toroidal resonances in the planar metasurface, the TASRs are arranged in mirrored configuration, separated by a distance of 15 μm, as shown in the microscopic image (Figure 1(b)) of the sample. The sample image shows that the TASRs are mirrored to each other along the Y-direction. The unit cell area with the periodicity of 150 μm × 75 μm is shown by the dotted rectangular curve, which on repetition along the XY-plane forms the planar toroidal metasurface. The metasurface is excited by the THz pulse at normal incidence, which has its electric field polarized parallel to the non-gap arm of TASR. Figure 1(c) shows the schematic of toroidal excitation in the unit cell of the metasurface due to the mirrored TASRs configuration. At the instant of toroidal resonance surface currents ($\vec{I}$) excited in the pair of TASRs are opposite in nature which confines the induced time varying magnetic field ($\vec{H}$) in a small circular region. This induced dynamic $\vec{H}$ field further induces the dynamic electric field ($\vec{E}$), as per the right hand rule points along the X-direction shown by the fictitious arrow of a toroidal dipole vector ($\vec{T_x}$). For sensing, when a photoresist layer of thickness t and refractive index (n) equal to 1.66 is spin coated on the top of the toroidal metasurface, as shown in Figure 1(d), a red shift in the frequency of toroidal resonance can be clearly observed, as depicted by the simulated amplitude transmission spectra of the metasurface in Figure 1(e). The simulated Q factor of the toroidal resonance is ~9.6, which indicates the sharpness of resonance near the resonance frequency. Even at larger degree of asymmetry in TASR, excited toroidal resonance is of sufficiently narrow linewidth and has a large amplitude, which allows to precisely detect the red shift in the resonance frequency during the experiments. Further to investigate the role of toroidal dipole in the sensing activity, the X-component of toroidal dipole has been calculated numerically near the spectral region of sharp resonance. In the presence of analyte medium, the T_x component versus frequency plot in Figure 1(f) clearly indicates the redshift in toroidal coupling between the mirrored resonators, which is responsible for the shift in toroidal resonance.

Planar toroidal metamaterials are spin coated with different thicknesses of photoresist. Profilometry was used to detect the thickness of the photoresist layer by the scratch method. Commercially available CST Microwave Studio was used to numerically simulate the coated metasurface response. Figure 2(a) shows the simulated amplitude transmission spectra of the toroidal metasurface where we observe red shifting of the toroidal resonance with increasing thickness of photoresist. Without the photoresist film ($t = 0$ μm), the toroidal dipole resonance first appears at the frequency of 0.402 THz. For the photoresist film thicknesses
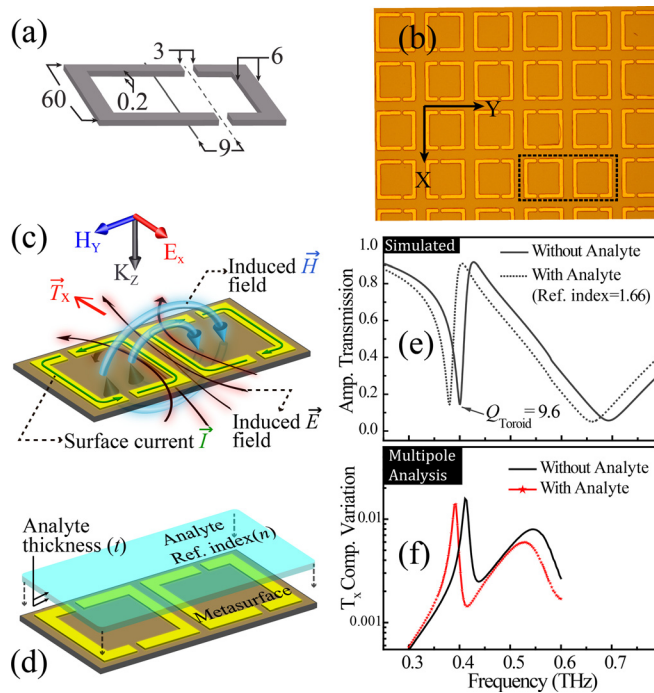

FIG. 1. High Q planar toroidal metasurface. (a) Dimensional features of the terahertz asymmetric split ring resonator (TASR) with all dimensions at a micron scale. (b) Microscopic image of toroidal metasurface along the XY-plane, with unit cell representation shown by the dotted rectangular curve. (c) Artistic impression of toroidal dipole generated due to the circulating magnetic field produced by surface currents induced in mirrored TASR configuration. (d) Unit cell of the toroidal metasurface coated with the analyte layer on the top. (e) Simulated frequency versus amplitude transmission spectra of the metasurface with and without the analyte layer. (f) Numerically calculated X-component of the toroidal dipole moment versus the frequency plot, via multipole analysis in the vicinity of toroidal resonance, for the case with and without the analyte layer on the metasurface.
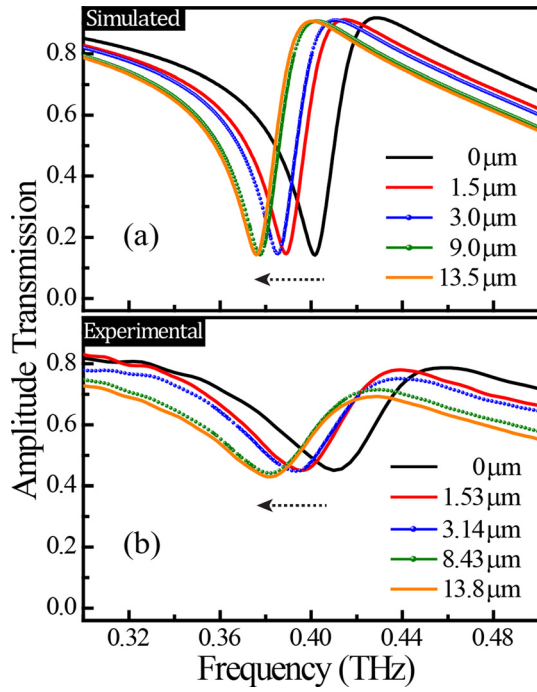
FIG. 2. The spectral shift in toroidal resonance. (a) Simulated and (b) experimentally measured amplitude transmission spectra with a different thickness of photoresist coated on the top of the metasurface. Dotted arrow pointing towards the left shows the shift in the frequency of toroidal resonance.
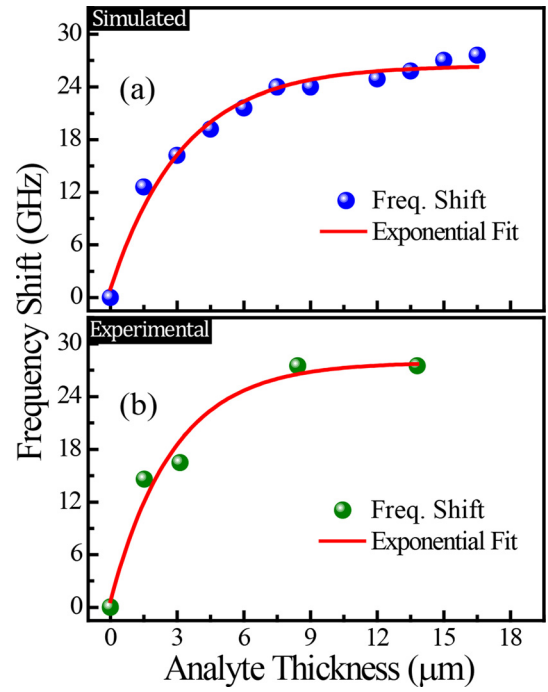

FIG. 3. The exponential fit for frequency shifts. (a) Simulated and (b) experimentally measured frequency shifts with the increase in the thickness of analyte (photoresist) layer. An exponential fit has been performed by the equation $f_{shift} = f_{sat} + A^* \exp(-R_0^* t)$, where t is the analyte thickness and f_{sat} is the maximum frequency shift at saturation point of fitted curve.

of 1.5, 3.0, 9.0, and 13.5 μm the toroidal resonances are gradually red shifted by 12.5, 16.2, 24.0, and 25.8 GHz, respectively. It is also evident that beyond the film thickness of 9 μm, the red shift in toroidal dipole resonance nearly saturates at the frequency 0.376 THz. Figure 2(b) shows the experimentally measured response that agrees well with the simulations. The red shift in the resonance frequency is mainly caused by the dielectric fill in the capacitive gaps of TASRs, which increases the net capacitance of TASRs and alters the resonance frequency. Also, fringing field effect at the capacitive gaps further plays a role in the red shift of toroidal resonance with an increase in the thickness of the photoresist layer. Once the penetration of fringing fields above certain height from the metasurface disappears, no shift is observed in the frequency of resonance even with the increase in the thickness of the photoresist layer.

Further to investigate the spatial extent of the fringing fields above the metasurface, we have plotted the frequency shift with respect to the analyte thickness. For the simulated response, Figure 3(a) shows the variation in frequency shifts along with the exponential fit as the thickness of analyte layer increases. The exponential fit curve nearly saturates beyond the thickness of 10 μm. This gives a fair idea of the penetration depth of fringing fields above the metasurface. Almost similar variation is observed for the measured response, as shown in Figure 3(b). Saturated frequency shift from the exponential fit curve for the measured response (27.9 GHz) differs by 1.5 GHz compared to the simulated response (26.4 GHz), which is lower than the frequency resolution of our measurements (16.6 GHz).

To experimentally determine the sensitivity for thin analyte layers, we coated a new set of samples with the 0.25 μm

thick layer of Silicon dioxide (SiO$_2$) and Germanium (Ge), due to high contrast in their refractive index. Table I shows the resonance frequencies and corresponding refractive index for the specific analyte material. To identify shift in toroidal resonance, the nitrogen (N$_2$) environment is used as the reference medium for both materials. A significant shift in the resonance frequency compared to N$_2$ environment can be observed in simulated (Figure 4(a)) and experimental (Figure 4(b)) transmission spectra for the thin analyte coatings of SiO$_2$ and Ge. For thin analyte films ($\sim$0.25 μm), the experimentally estimated value of sensitivity from Figure 4(c) is found to be around 6 GHz/refractive index unit (RIU), which matches well with simulated results (inset plot). This lower sensitivity value is for the ultrathin 250 nm thickness of the analyte. The equivalent sensitivity per micron of thickness of the analyte is 24 GHz/RIU.

We also analyzed the sensitivity of the toroidal resonance for sufficiently thick analyte layers by varying the refractive index (n) of the analyte layer to be sensed. Figure 5(a) shows the shift in the resonance frequency of simulated toroidal dipolar response with an increase in the refractive index (n) of the constant thick (4 μm) analyte layer. The variation in frequency shifts (as shown in Figure 5(b)) appears to

TABLE I. Table depicting experimental resonance frequency of toroidal metasurface in the presence of corresponding refractive index analyte medium (N$_2$, SiO$_2$, Ge) on metasurface.

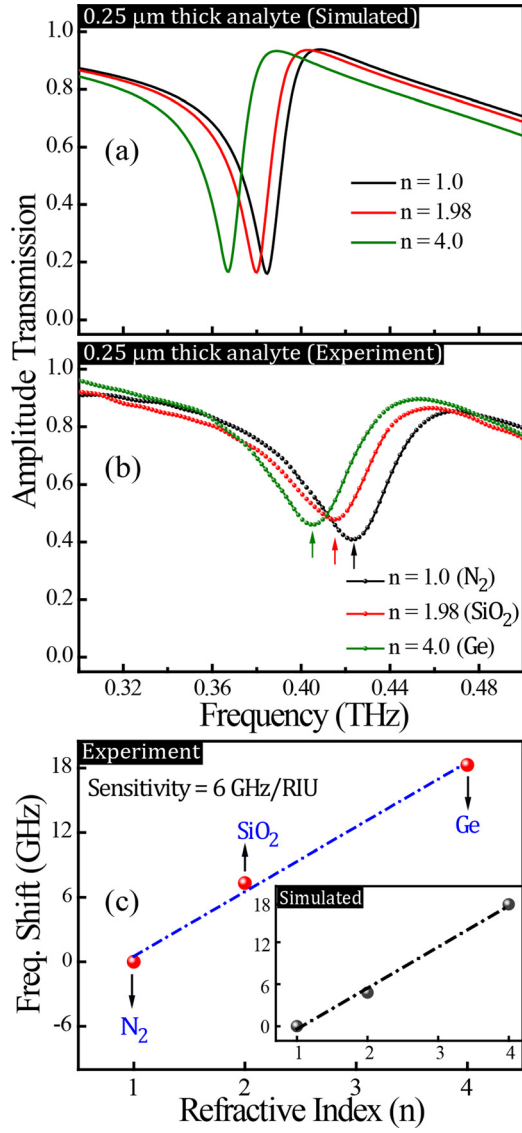| Analyte on metasurface	Resonance frequency (GHz)	Refractive index (n)
Nitrogen (N$_2$)	422.6	1
0.25 μm thick SiO$_2$ layer	415.3	1.98
0.25 μm thick Ge layer	404.3	4

FIG. 4. The sensitivity of the 0.25 μm ultrathin analyte layer. (a) Simulated and (b) experimentally measured amplitude transmission spectra showing the shift in toroidal resonance with different analytes, where nitrogen (N$_2$) environment is used as a reference medium for a 0.25 μm thick analyte layer of silicon dioxide (SiO$_2$) and germanium (Ge) coated on the top of the metasurface. (c) Resonance frequency shift versus refractive index plot for samples coated with SiO$_2$ and Ge. For thin analyte films, linear fit has been performed to determine the sensitivity (slope) of the metasurface.

be linear in nature, so we performed linear fit to determine the sensitivity, which turns out to be 27.3 GHz/RIU. The measure of sensitivity value is estimated in terms of wavelength ($\Delta\lambda$) per RIU, which is given by the equation $\left|\frac{d\lambda}{dn}\right| = \frac{c}{f_o^2} * \frac{df}{dn}$, where c is the speed of light, f_o is the resonance frequency, and n represents the refractive index of the analyte. In terms of $\Delta\lambda$/RIU, the sensitivity value that we have obtained for the toroidal metasurface coated with 4 μm thick layer of analyte is 4.88×10^4nm/RIU. The sensitivity values of the planar toroidal metasurface are lower compared to previously reported values of the Fano resonators array.[9] Moreover, to probe the analyte and substrate thickness dependent sensitivity of the toroidal metasurface, we calculated sensitivities for different thicknesses of the analyte layer for the toroidal metasurface on silicon (Si) and mylar substrates. Figure 6(a) shows the sensitivity plot for the
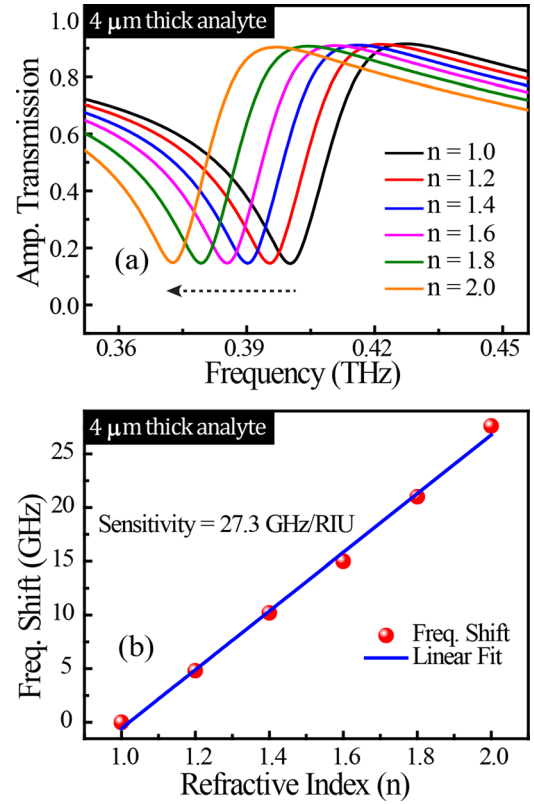

FIG. 5. The sensitivity of toroidal resonance. Simulated (a) red shifted amplitude transmission spectra, and correspondingly derived (b) frequency shift vs refractive index plot for the 4 μm thick analyte layer, with an increasing refractive index, coated on the toroidal metasurface. Linear fit has been performed to determine the sensitivity of the metasurface.

increasing thickness of analyte layer coated on the toroidal metasurface on 25 μm thick Si and mylar substrates. Mylar substrate gives better sensitivity compared to the Si substrate due to the lower refractive index of mylar. We note that the sensitivity of toroidal resonance increases and subsequently saturates with an increase in the thickness of the analyte layer. The maximum sensitivity for the toroidal metasurface is found to be 41 GHz/RIU (7.32×10^4nm/RIU) for the Si substrate and 186 GHz/RIU (10.3×10^4nm/RIU) for the mylar substrate. The sensitivity plot nearly tends to saturate beyond the 13 μm thick analyte layer. Finally, to probe the effect of substrate thickness on sensitivity, simulations have been performed for the toroidal metasurface patterned on different thicknesses of the substrates (Si, mylar), and coated with a 4 μm constant thickness of the analyte layer. As shown in Figure 6(b), the sensitivity decays exponentially with an increase in the thickness of the substrate and nearly saturates beyond the substrate thickness of 20 μm.

In brief, we demonstrate that toroidal resonances in planar metamaterials could be used as a platform for sensing applications. We have experimentally demonstrated high-Q sensing via sharp toroidal resonance at the terahertz spectral range. High resolution terahertz measurements allow us to measure the minute shift in the resonance frequencies as ultrathin layers of dielectric film were coated on top of the toroidal metasurface. Compared to other sharp resonances in metamaterials, toroidal dipole resonance offers better sensitivity at larger asymmetry in TASRs, despite short scan duration on the time scale. The impact of our work lies in
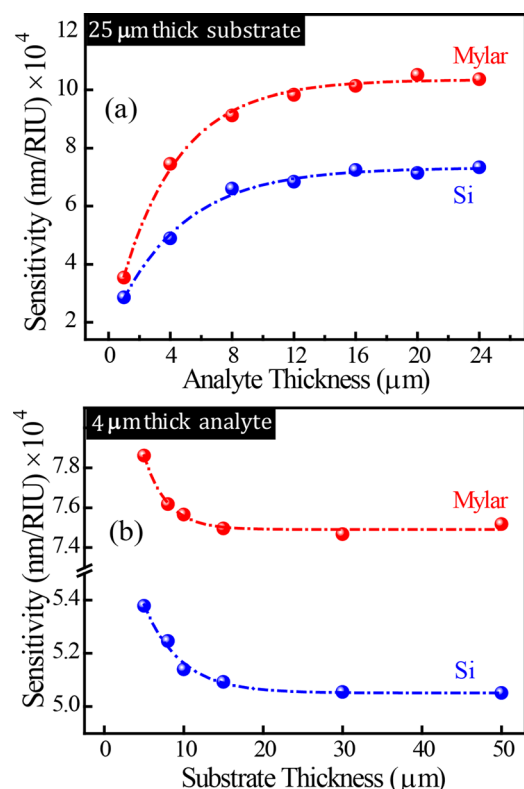
FIG. 6. The sensitivity of toroidal resonance with variation in the substrate thickness and analyte thickness. (a) Simulated sensitivities plot with the analyte layer of different thicknesses with the varying refractive index coated on the toroidal metasurface fabricated on 25 μm thick silicon (Si) and mylar substrates. (b) the 4 μm thick analyte layer of varying refractive indexes coated on the metasurface patterned on the substrates (Si, Mylar) with the increasing thickness. Exponential fit (dotted curve) performed to determine the maximum sensitivity value that could be achieved for the toroidal metasurface in all cases.

identifying the high-*Q* terahertz toroidal metasurface based sensing that would drive the path for innovative designs and realization of photonic devices for dielectric, chemical, and biomolecular sensing with spectral signatures in the terahertz regime.

[1] J. B. Pendry, A. J. Holden, D. J. Robbins, and W. J. Stewart, IEEE Trans. Microwave Theory Techn. **47**, 2075 (1999).
[2] T. J. Yen, W. J. Padilla, N. Fang, D. C. Vier, D. R. Smith, J. B. Pendry, D. N. Basov, and X. Zhang, Science **303**, 1494 (2004).
[3] N. I. Zheludev, S. L. Prosvirnin, N. Papasimakis, and V. A. Fedotov, Nat. Photonics **2**, 351 (2008).
[4] N. I. Zheludev and Y. S. Kivshar, Nat. Mater. **11**, 917 (2012).
[5] V. M. Shalaev, Nat. Photonics **1**, 41 (2007).
[6] C. M. Soukoulis, M. Kafesaki, and E. N. Economou, Adv. Mater. **18**, 1941 (2006).
[7] Y. Liu and X. Zhang, Chem. Soc. Rev. **40**, 2494 (2011).
[8] D. Schurig, J. J. Mock, B. J. Justice, S. A. Cummer, J. B. Pendry, A. F. Starr, and D. R. Smith, Science **314**, 977 (2006).
[9] R. Singh, W. Cao, I. Al-Naib, L. Cong, W. Withayachumnankul, and W. Zhang, Appl. Phys. Lett. **105**, 171101 (2014).
[10] J. N. Anker, W. P. Hall, O. Lyandres, N. C. Shah, J. Zhao, and R. P. Van Duyne, Nat. Mater. **7**, 442 (2008).
[11] G. Dayal, X. Y. Chin, C. Soci, and R. Singh, Adv. Opt. Mater. **4**, 1295 (2016).
[12] I. Al-Naib, C. Jansen, and M. Koch, Appl. Phys. Lett. **93**, 083507 (2008).
[13] A. Boltasseva and H. A. Atwater, Science **331**, 290 (2011).
[14] V. A. Fedotov, M. Rose, S. L. Prosvirnin, N. Papasimakis, and N. I. Zheludev, Phys. Rev. Lett. **99**, 147401 (2007).
[15] R. Singh, I. Al-Naib, W. Cao, C. Rockstuhl, M. Koch, and W. Zhang, IEEE Trans. Terahertz Sci. Technol. **3**, 820 (2013).
[16] S. Xiao, V. P. Drachev, A. V. Kildishev, X. Ni, U. K. Chettiar, H.-K. Yuan, and V. M. Shalaev, Nature **466**, 735 (2010).
[17] I. Al-Naib, R. Singh, C. Rockstuhl, F. Lederer, S. Delprat, D. Rocheleau, M. Chaker, T. Ozaki, and R. Morandotti, Appl. Phys. Lett. **101**, 071108 (2012).
[18] I. Al-Naib, E. Hebestreit, C. Rockstuhl, F. Lederer, D. Christodoulides, T. Ozaki, and R. Morandotti, Phys. Rev. Lett. **112**, 183903 (2014).
[19] R. Singh and N. I. Zheludev, Nat. Photonics **8**, 679 (2014).
[20] D. Ye, K. Chang, L. Ran, and H. Xin, Nat. Commun. **5**, 5841 (2014).
[21] N. Liu, M. L. Tang, M. Hentschel, H. Giessen, and A. P. Alivisatos, Nat. Mater. **10**, 631 (2011).
[22] N. Liu, T. Weiss, M. Mesch, L. Langguth, U. Eigenthaler, M. Hirscher, C. Sönnichsen, and H. Giessen, Nano Lett. **10**, 1103 (2010).
[23] E. Cubukcu, S. Zhang, Y.-S. Park, G. Bartal, and X. Zhang, Appl. Phys. Lett. **95**, 043113 (2009).
[24] T. Driscoll, G. O. Andreev, D. N. Basov, S. Palit, S. Y. Cho, N. M. Jokerst, and D. R. Smith, Appl. Phys. Lett. **91**, 062511 (2007).
[25] H. Tao, L. R. Chieffo, M. A. Brenckle, S. M. Siebert, M. Liu, A. C. Strikwerda, K. Fan, D. L. Kaplan, X. Zhang, R. D. Averitt, and F. G. Omenetto, Adv. Mater. **23**, 3197 (2011).
[26] M. Tonouchi, Nat. Photonics **1**, 97 (2007).
[27] B. Ferguson and X.-C. Zhang, Nat. Mater. **1**, 26 (2002).
[28] S. H. Lee, J. Choi, H.-D. Kim, H. Choi, and B. Min, Sci. Rep. **3**, 2135 (2013).
[29] T. Chen, S. Li, and H. Sun, Sensors (Basel, Switzerland) **12**, 2742 (2012).
[30] X. Xu, B. Peng, D. Li, J. Zhang, L. M. Wong, Q. Zhang, S. Wang, and Q. Xiong, Nano Lett. **11**, 3232 (2011).
[31] X. Liu, S. MacNaughton, D. B. Shrekenhamer, H. Tao, S. Selvarasah, A. Totachawattana, R. D. Averitt, M. R. Dokmeci, S. Sonkusale, and W. J. Padilla, Appl. Phys. Lett. **96**, 011906 (2010).
[32] T. Kaelberer, V. A. Fedotov, N. Papasimakis, D. P. Tsai, and N. I. Zheludev, Science **330**, 1510 (2010).
[33] M. Gupta, V. Savinov, N. Xu, L. Cong, G. Dayal, S. Wang, W. Zhang, N. I. Zheludev, and R. Singh, Adv. Mater. **28**, 8206 (2016).
[34] Y. Fan, Z. Wei, H. Li, H. Chen, and C. M. Soukoulis, Phys. Rev. B **87**, 115417 (2013).
[35] A. A. Basharin, V. Chuguevskiy, N. Volsky, M. Kafesaki, and E. N. Economou, Phys. Rev. B **95**, 035104 (2017).
[36] M. Gupta and R. Singh, Adv. Opt. Mater. **4**, 2119 (2016).
[37] V. Savinov, V. A. Fedotov, and N. I. Zheludev, Phys. Rev. B **89**, 205112 (2014).
[38] N. Papasimakis, V. A. Fedotov, V. Savinov, T. A. Raybould, and N. I. Zheludev, Nat. Mater. **15**, 263 (2016).
[39] S. Han, L. Cong, F. Gao, R. Singh, and H. Yang, Ann. Phys. **528**, 352 (2016).
[40] B. Luk'yanchuk, N. I. Zheludev, S. A. Maier, N. J. Halas, P. Nordlander, H. Giessen, and C. T. Chong, Nat. Mater. **9**, 707 (2010).
[41] H. Tao, A. C. Strikwerda, M. Liu, J. P. Mondia, E. Ekmekci, K. Fan, D. L. Kaplan, W. J. Padilla, X. Zhang, R. D. Averitt, and F. G. Omenetto, Appl. Phys. Lett. **97**, 261909 (2010).
[42] J. F. O'Hara, R. Singh, I. Brener, E. Smirnova, J. Han, A. J. Taylor, and W. Zhang, Opt. Express **16**, 1786 (2008).
[43] J. Burgin, M. Liu, and P. Guyot-Sionnest, J. Phys. Chem. C **112**, 19279 (2008).
[44] M. S. Lavine, Science **346**, 50 (2014).
[45] B. Ng, S. M. Hanham, V. Giannini, Z. C. Chen, M. Tang, Y. F. Liew, N. Klein, M. H. Hong, and S. A. Maier, Opt. Express **19**, 14653 (2011).
[46] B. Reinhard, K. M. Schmitt, V. Wollrab, J. Neu, R. Beigang, and M. Rahm, Appl. Phys. Lett. **100**, 221101 (2012).
[47] J. Li, Z. Tian, Y. Chen, W. Cao, and Z. Zeng, Appl. Opt. **51**, 3258 (2012).